A Multichannel Model for the Self-Consistent Analysis of Coherent Transport in Graphene Nanoribbons

Davide Mencarelli, Luca Pierantoni, Marco Farina, Andrea Di Donato, and Tullio Rozzi*

Dipartimento di Ingegneria Biomedica Elettronica e Telecomunicazioni, Università Politecnica delle Marche, Via Brecce Bianche, 60100 Ancona, Italy

Its extremely high carrier mobility, thermal conductivity, and ballisticity of charge transport make graphene (*i.e.*, a monolayer of hexagonal carbon lattice) an excellent candidate for achieving the high speed and high performance of the next generation RF electronics at the nanoscale, including field-effect transistors (FET), frequency multipliers, interconnects, sensors, and wireless devices.

Our analysis is focused on graphene nanoribbon (GNR), that is, a narrow strip of graphene.[1-7] The analysis of quantum transport in GNR is carried out by a variety of models, such as tight binding (TB), effective mass, and $k \cdot p$ approximations; the latter yields a Dirac-like system of equations,[8] which is effectively applied to large GNRs. Two main methods stem from the TB approach: the first one makes use of Green's function of a GNR region;[9-11] the second one represents an alternative formulation to the technique of ref 12, where a monatomic lattice is subdivided into layers perpendicular to the transport direction, and use is made of a multimode scattering matrix model. These techniques provide insight on the effects on quantum transport of applied external electric and magnetic fields,[13] bendings,[14] discontinuities,[10] and edge terminations.[15] The underlying assumptions are the ballisticity of transport and the weakness of the interaction between charges, due to the relatively long distances involved.

The study of GNRs typically involves two physical ports (input and output), whereas in our previous approach,[16] multiport GNR circuits can be considered. Each port, seen as the termination of a semi-infinite GNR waveguide, is described by means of a basis of electronic eigenfunctions. In this contribution, important steps forward have been made with respect to ref 16, where calculation is not self-consistent: in particular, we introduce a full self-consistent analysis of

ABSTRACT In this contribution, we analyze the multichannel coherent transport in graphene nanoribbons (GNRs) by a scattering matrix approach. We consider the transport properties of GNR devices of a very general form, involving multiple bands and multiple leads. The 2D quantum transport over the whole GNR surface, described by the Schrödinger equation, is strongly nonlinear as it implies calculation of self-generated and externally applied electrostatic potentials, solutions of the 3D Poisson equation. The surface charge density is computed as a balance of carriers traveling through the channel at all of the allowed energies. Moreover, formation of bound charges corresponding to a discrete modal spectrum is observed and included in the model. We provide simulation examples by considering GNR configurations typical for transistor devices and GNR protrusions that find an interesting application as cold cathodes for X-ray generation. With reference to the latter case, a unified model is required in order to couple charge transport and charge emission. However, to a first approximation, these could be considered as independent problems, as in the example.

KEYWORDS: graphene nanoribbon · coherent transport · scattering matrix · X-ray cathode · field-effect transistor

the transport equation and of the electrostatic potential generated by the GNR charge density. As it will be shown, this is obtained by numerical iteration. The net charge density in the GNR is obtained by considering the contribution of all occupied states, that is, from the bottom energies up to the Fermi level that can also comprise, differently from ref 16, bound electronic states. This is a nontrivial development because, usually, the transport analysis is restricted to one or a few wave functions and to low carrier energies; for example, the current through a monodimensional channel for small bias voltages is usually limited by the number of free states around the Fermi energy. Similarly, the computational load, in the analysis of n-doped (p-doped) GNRs, is often reduced by considering contributions to the current just from the conduction band electrons (or valence band holes). However, the above simplification may be unsuitable, as highlighted in a later example, in the cases of strong localized perturbations of the GNR potential, with respect to the

band gap; the same holds in the case of abrupt GNR terminations.

The last case is of particular interest for field-emission applications: we will show that the presence of bound electrons in correspondence with a GNR termination leads to strong charge concentrations. The problem is, to some extent, similar to that of the screening effect of localized charges in a 2DEG, with some more difficulties arising from the finite width of the GNR and from the constraints to the electrostatic potential due to the metal electrodes.

In Figure 1, the above-mentioned scheme of multiport GNR-FET is shown. Recently, a full quantum solver for carbon nanotube (CNT)-FET, with a user-friendly interface, has been developed:[17] a first version will be available online, and corresponding software is being developed for simulation of a GNR-FET. New ultraminiaturized devices with potential medical applications may also be considered, for example, GNR-based cold cathode, to be used in place of the traditional thermionic X-ray sources for standard tomography. In fact, CNTs are already being employed for this purpose; the elimination of the resistively heated metal filaments greatly extends the working life of X-ray tubes; moreover, the power requirements of the new X-ray nanosource can be reduced efficiently to allow portable X-ray machines. It may be natural to wonder whether GNR planar structures could behave as better field emitters than CNTs or graphene sharp extrusions.[18] The following considerations point to this direction, namely, (i) due to the planar geometry, good metal contacts may be obtained; (ii) densely packed states are present in the case of zigzag GNRs; this may possibly lead to increased field emission; (iii) GNR-FET configurations could allow control of the charge resonances in the GNR; (iv) in principle, a proper choice of the GNR pattern may provide amplification and adjustable orientation of the emitted charge, owing to the "array factor".

Many simplified models, such as the Fowler–Nordheim relation,[19] are currently applied to the problem of field emission by sharp tips. Differently from these heuristic models, our approach allows, in principle, the investigation of the coupling between the internal problem of quantum transport in GNR and the "antenna" problem of the emission, consistent with the self-generated potential.

Model. Let us start from the discrete formulation[16] of the Schrödinger equation

$$H_l\psi_l + H_0\psi + H_r\psi_r = E\psi \quad (1)$$

where E is the energy, ψ_l, ψ, and ψ_r are the wave functions of three consecutive GNR unit cells, and the Hamiltonian has been decomposed in three matrices which model transfer energies between adjacent cells: matrix H_l (H_r) includes the hopping elements from a unit cell to the previous (following) one, H_0 is the self-energy matrix of the unit cell. The relations $H_l = H_r^+$ and
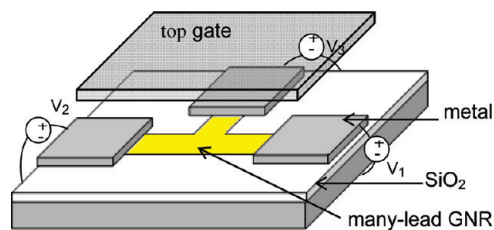
Figure 1. Many-lead GNR-FET: a T-shaped GNR is shown. $V_{1,2,3}$ are metal electrodes.

$H_0 = H_0^+$ hold. The diagonal elements of H_0 contain the electrostatic potential solution of Poisson's equation. Solution of eq 1 provides the basis of the eigenmodes of the GNR. Exploiting periodicity, eq 1 becomes

$$(H_l e^{jkL} + H_0 + H_r e^{-jkL})\psi = E\psi,$$
$$\psi = e^{-jky}\sum_i \psi_i \delta(x - x_i, y - y_i) \quad (2)$$

where i spans the unit cells, k is the wavenumber, and L is the length of the unit cell. The solutions of eq 2, corresponding to different branches of the dispersion curves, can be distinguished as propagating modes for real k and evanescent modes for complex or imaginary k. In order to provide the correct mode normalization, wave functions have to be divided by[16]

$$A = \sqrt{\frac{f_T(E)}{4\pi \mathrm{Im}(\psi^+ H_r e^{-jkL}\psi)}} \quad (3)$$

where f_T is the Fermi distribution function at T temperature. The above normalization implies that all propagating modes carry the same current with reference to Landauer's formula. It also ensures charge neutrality as verified in the following. Assuming $kL = \theta$ and taking the partial derivative of eq 2, we have

$$\partial_\theta(H_l e^{j\theta} + H_0 + H_r e^{-j\theta})\psi = j(H_l e^{j\theta} - H_r e^{-j\theta})\psi$$
$$- (H_l e^{j\theta} + H_0 + H_r e^{-j\theta})\frac{jy}{L}\psi = \partial_\theta E\psi - E\frac{jy}{L}\psi$$

the above expression is simplified by using eq 2 and then premultiplied by ψ^+, yielding

$$j\psi^+\circ(H_l e^{jkL} - H_r e^{-jkL})\psi = 2\mathrm{Im}\,\psi^+\circ(H_r e^{-jkL})\psi$$
$$= \partial_\theta E\psi^+\circ\psi$$

where the scalar product gives a number, that is, the total charge and not a charge density spatial vector, as it implies spatial summation. The last result is used to evaluate the energy integral of the charge associated with any wave function (corresponding to one of the N branches of the dispersion curves of a N atom unit cell[16]), expressing charge neutrality

$$2\int \frac{\psi^+\circ\psi}{4\pi\mathrm{Im}[\psi^+(H_r e^{-jkL})\psi]}\,dE$$
$$= 2\int_0^{2\pi} \frac{\psi^+\circ\psi}{4\pi\mathrm{Im}[\psi^+(H_r e^{-jkL})\psi]}\frac{2\mathrm{Im}[\psi^+\circ(H_r e^{-jkL})\psi]}{\psi^+\circ\psi}\,d\theta$$
$$= 2 \quad (4)$$

where the normalization (eq 3) with $T \sim 0$ has been used, and the factor 2 accounts for spin degeneracy. If the integration (eq 4) is restricted to the range from the bottom energy up to the Dirac point, placed in the middle of the interval of allowed energies, and assumed as zero reference, then the result is 1, that is, one electron per atom.

The scattering matrix of a GNR device, defined as in ref 16, relates incident and reflected mode amplitudes at port sections, which are different terminations of a many-lead GNR circuit. For instance, for a two-port device, we have

$$\begin{bmatrix} b_1 \\ b_2 \end{bmatrix} = \begin{bmatrix} S_{11} & S_{12} \\ S_{21} & S_{22} \end{bmatrix} \begin{bmatrix} a_1 \\ a_2 \end{bmatrix} \qquad b_1\overleftarrow{\psi}_1 + a_1\overrightarrow{\psi}_1 \;\longrightarrow\; \boxed{S} \;\longrightarrow\; a_2\overleftarrow{\psi}_2 + b_2\overrightarrow{\psi}_2$$

where the arrows indicate the propagation direction of carriers.

One of the difficulties of the proposed method resides in that the scattering formulation has to be adapted to a periodic waveguide, where the right basis to be used for describing charge transport is given by the complete set of Floquet, or periodic, modes. Within the latter choice, the scattering parameters can be shown to obey, for example, the expected reciprocity and losslessness constraints, respectively

$$S = S^T \text{ and } S^+S = I$$

The number of modes at any port depends on the port size, on the Fermi level, and on GNR chirality. Regressive modes, either above or below cutoff, are scattered out of the GNR without reflection: this means perfectly transparent ports.

A coherent application of the proposed scattering model to GNR transitions and discontinuities implies computing the incidence, reflection, and mutual coupling of any wave function, with a proper weight given by Fermi probability. Propagation of charges is based on their position on the dispersion curves: positive (negative) group velocity dE/dk means progressive waves, moving from left to right (from right to left). The sign of the group velocity for any wave function corresponds to the sign of its associated current.

In case of a two-port GNR, the charge density is obtained by summing the normalized wave functions of carriers injected from the two opposite ports:

$$Q_c = -e \sum_i \int \left(f_1(E) \frac{|\psi_1^i(x, y, E)|^2}{A^2} + f_2(E) \frac{|\psi_2^i(x, y, E)|^2}{A^2} \right) dE \tag{5}$$

where the subscript "c" refers to the continuous integral operation, the upper index "i" of $\psi_{1,2}^i$ indicates the ith band, whereas the lower ones indicate the ports; f_1 and f_2 are the Fermi probabilities for the electrons at ports 1 and 2, respectively, and $e = 1.6 \times 10^{-19}$C.

For a multiport device, all physical quantities are obtained by including the charge contributions from all ports. For instance, the total current flowing through

the pth port includes contribution of all modes transmitted from the port p to all the other ports:

$$I_p = \frac{2e}{h} \sum_{i, j, q} \int (f_p(E) - f_q(E)) S_{pq}^{i,j}(E) dE \tag{6}$$

where $S_{pq}^{i,j}$ is the scattering coefficient from mode i to mode j, and from port p to port q.

Validation Test Cases. In this subsection, we discuss some preliminary results. They are needed, on the one hand, to show in concrete the typical issues we are dealing with and, on the other, to test accuracy and numerical consistence/robustness of the applied method.

First of all, the integral (eq 5) has been performed all over the energy states below the Dirac point ($E = 0$) of a semiconducting 32 atom GNR standing on air. In each atomic position, the resulting total charge has to be equal to 1 in order to compensate for the positive unit charges of the atomic sites: this is achieved, provided that the integration step is sufficiently small.

When an external potential is applied, in the form of a positive spatial pulse along the GNR axis, of amplitude *much smaller than the band gap*, charge neutrality is still recovered, as long as the contribution of bound states is included. In this case, in fact, the continuous integral (eq 5) has to be completed by a discrete spectrum representing confined modes. The superimposed potential well yields bound electronic states that exactly compensate the reduced charge penetration in the well region, in such a way that charge neutrality is guaranteed everywhere. The discrete contribution Q_d to the total charge density is given by

$$Q_d = -e \sum_i |\psi(x, y, E_i)|^2 \tag{7}$$

where each wave function is now just normalized to 2 after integration over the whole GNR volume; neutrality in fact means zero value of the net charge Q, given by

$$Q = (Q_c + Q_d) + e \sum_j \delta(x - x_j, y - y_j) = 0 \tag{8}$$

Let us consider, as a more interesting example, the case of a potential well *deeper than the band gap*: in particular, a finite potential pulse of 0.125 V is applied to a 16 atom armchair GNR, having a vanishing band gap. In this case, charges tend to "fill" the potential well and the neutrality is locally lost. This is usually described by assuming a uniform Fermi level, as depicted in Figure 2a. Even without considering charge interaction—we will consider it later—the above simplification does not account correctly for local scattering effects. The contributions of the confined modes of Q_c and of Q_d are shown, respectively, in Figure 2b—d. The two surface plots of Figure 2e compare the net charge obtained respectively by the scattering method, that is, Q from eq 8, and by a direct evaluation exploiting Fermi level alignment: scattering enhances the effect of the potential
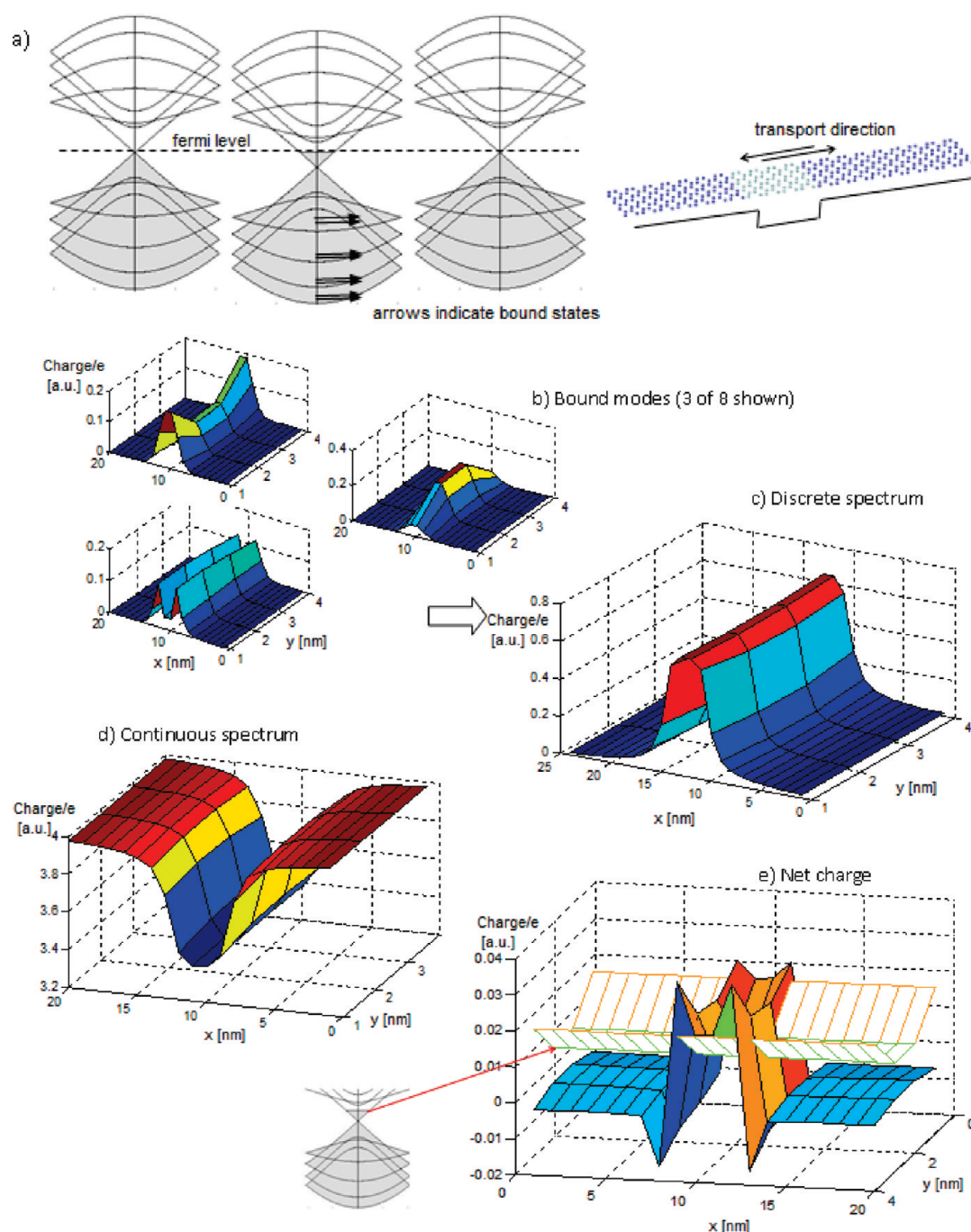
Figure 2. (a) Dispersion curves (left) of simulated GNR and potential well (right); (b) three of the eight confined modes; (c) Q_d, sum of all bound modes; (d) continuous integral Q_c; (e) GNR net charge; the red arrow points to a uniformly charged GNR, reported for comparison.

pulse where it changes rapidly, namely, the appearance of charge ripples. Note that each point of the curves of Figure 2b—e comprises the charges of four close atomic sites.

As it has been observed,[20] confinement of charge propagating in graphene is not feasible by an applied electric potential, as, for instance, a potential barrier could be penetrated by electron/holes owing to net interaction with the occupied states below the barrier. This can be seen as an equivalent formulation of the

Klein paradox; by the same argument, one can explain the failure of an external electric field in confining charges in GNR. This situation is shown in Figure 3, where we consider zigzag GNRs with an externally applied voltage V_0, uniform along the GNR axis but varying in the transverse direction. In the upper part of the figure, we compare the wave functions of a 32 atom GNR (~3.4 nm wide), where V_0 is constant and $E - V_0 = 1.5$ eV, with those of a 64 atom GNR, where $E - V_0 = 1.5$ eV in the central 32 atoms and $E - V_0 = 0$ eV in the remaining
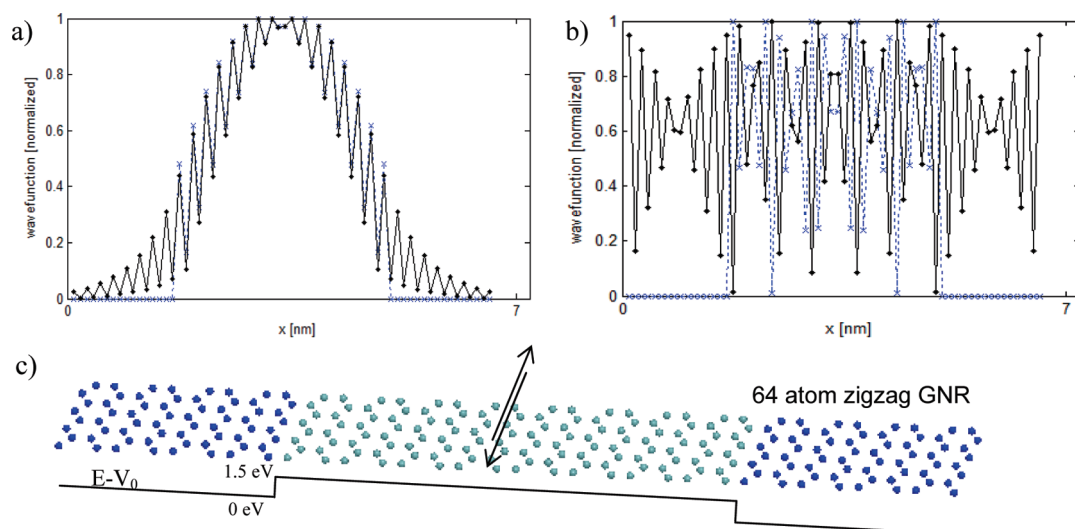
Figure 3. (a) First mode (dashed) of a 32 atom GNR with $E - V_0 = 1.5$ eV and first mode (solid) of a 64 atom GNR with $E - V_0$ as in (c); (b) third mode (dashed) of a 32 atom GNR with $E - V_0 = 1.5$ eV and third mode (solid) of a 64 atom GNR with $E - V_0$ as in (c); (c) transverse potential energy seen by the carriers; arrows indicate transport direction.

16 atoms at both sides, as shown in Figure 3c. Figure 3a shows that the first mode of the 64 atom GNR is laterally confined by this transverse stepwise potential, and its spatial distribution is similar to the first mode of the 32 atom GNR. This does not hold for all of the other modes; for instance, the external potential cannot play the role of a laterally guiding barrier for the mode shown in Figure 3b.

On the basis of the above observations, all modes have to be considered at any port because we do not know in advance which of them will contribute to charge transport.

EXAMPLES AND RESULTS

Some examples of self-consistent analysis of GNR under the influence of an external potential are shown in the following. The first one is constituted by a GNR-FET that is treated as a two-port circuit. The second one consists of a GNR protrusion that sticks out of a metal electrode over a dielectric substrate, modeled as a one-port circuit. In a third example, we report results on physical observables such as the electric current flowing through a GNR.

In the present work, the GNR is possibly deviated from its unperturbed state by the two following reasons: (i) the presence of an external applied potential; (ii) the fact that the GNR on the metal may have occupation function asymmetric with respect to the Dirac point: work functions of metal and GNR may be different, leading to a sort of GNR doping.[16] With reference to the second type of perturbation, the Fermi level of the contacted GNR has been chosen slightly away from the symmetry point of the dispersion curves, leading to a nonzero charge density. The latter is a free parameter resulting, in practice, from the contact with metal, doping, or impurities: self-consistency of the analysis

still holds because the charge density of the GNR over the metal could be, in principle, measured or estimated.

GNR-FET. Figure 4 shows a two-port GNR (standing on air) made of $n \cdot m = 16 \times 184$ atoms. The letters n and m indicate the number of atoms of the protruding GNR edge in x- and y-directions, respectively. Two finite pieces of GNR, extended beyond the ports in order to improve transparency, are included in the model. In order to expedite the numerical calculation, we assume infinitely thick electrodes, namely, the walls of a uniform rectangular waveguide (of course the walls are electrically isolated each other): two opposite walls act as source and drain, with potential constrained to voltages V_s and V_d, the other two walls act as side gates, with voltage V_g. This is shown in Figure 4a. The electrostatic potential is calculated by mode-matching at the planar interface containing the GNR; the matched modes are given by the attenuating electrostatic modes of the two semi-infinite rectangular waveguides, upper and lower half spaces, separated by the GNR plane. The charge density on the GNR affects mode-matching by compensating for the discontinuity of the potential derivative in the direction orthogonal to the GNR (z axis).

In the present example, the carrier density in the contacted GNR is assumed to be $\sim 6.8 \times 10^{12}$ cm^{-2} and external voltages are set to zero. It is remarked that the carrier density constitutes one of the main parameters affecting the calculation; in general, the higher the density, the higher the potential change and the slower the numerical convergence.

Potential and charge, at the last iterative step, are shown in panels b and c of Figure 4, respectively. The bottom part of the figure, Figure 4d, shows some iterations of the potential calculation; the solution converges
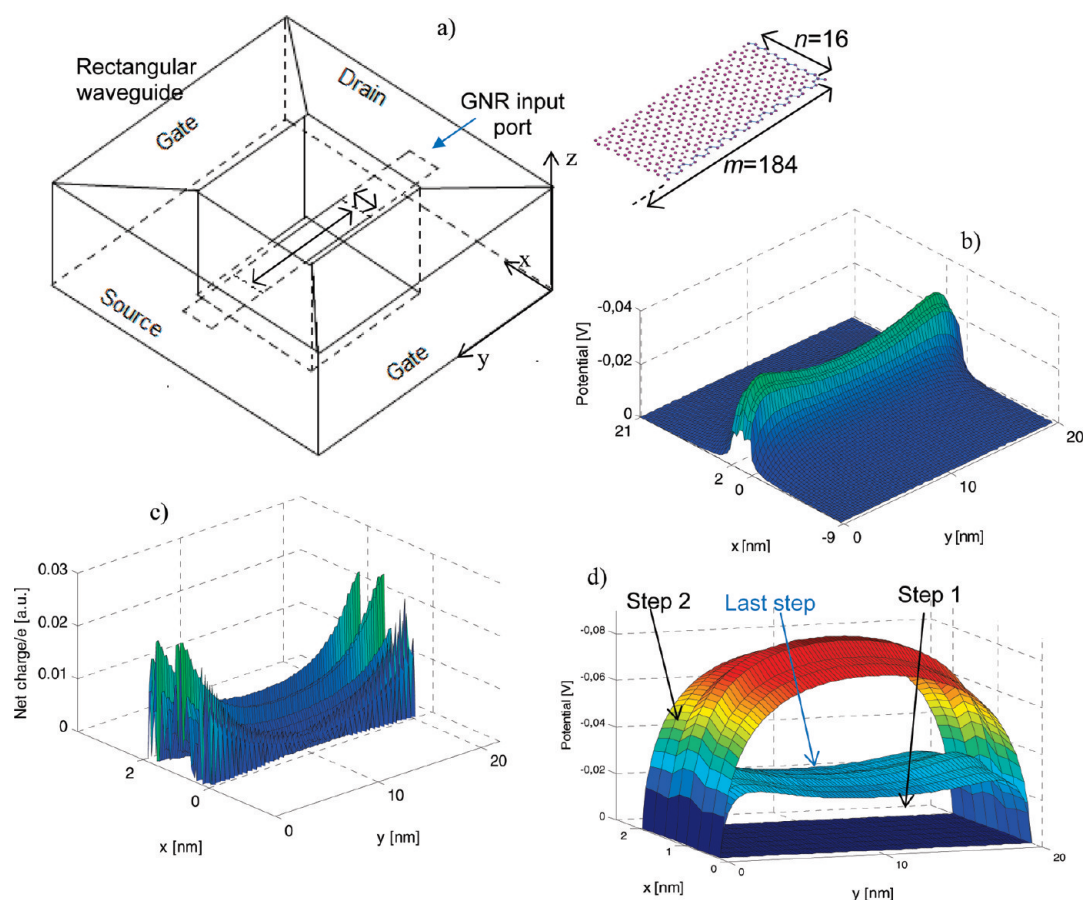
Figure 4. Simulation details: $n = 16$, $m = 184$, $V_g = 0$ V, $V_d = 0$ V, $V_s = 0$ V; Fermi level of contacted GNR = 0.29 eV, $T \sim 0$; (a) simulated structure; (b) potential in the plane of the GNR; (c) net charge in the suspended GNR. (d) Potential in the suspended GNR, at three iteration steps.

rapidly to the final curve, pointed by the arrow labeled with "last step". As a matter of fact, one of the features of our approach is given by its flexibility in simulating complex GNR devices, with a reasonably short simulation time. This is a crucial point as, in general, numerical convergence could require many iterations of the charge and potential equations. Convergence means that the potentials (or charge) at two consecutive steps differ by a very small amount at any spatial point, for example, less than 1% of their value. In Figure 4d, the last step is given by the tenth iteration.

Moreover, the model nonlinearity requires high numerical accuracy of the related calculation. For example, a dense refinement of energy states is needed because charge calculation implies an energy integration.[17] In Figure 4, the electronic charge is computed by fixing the energy resolution at 0.5 meV. An adaptive energy refinement (i.e., proportional to the slope of charge as a function of energy) has also been implemented, but it is not strictly necessary in the case considered, owing to the lack of strong electronic resonances.

GNR Protrusion. Figure 5a shows the details of the simulated structure; the substrate that completely fills the half space below the protruding GNR, is made of

SiO_2, with relative dielectric constant ~ 4; empty space is assumed above the plane of the GNR.

In Figure 5b, we report the potential in the plane of the GNR delimited by the metal walls after numerical convergence of the iterative Schrödinger–Poisson system. Charge injected in the protruding GNR affects the potential locally, and this in turn affects charge injection. Figure 5c shows the net charge in the protruding GNR, calculated using the one-port version of eqs 5, 7, and 8.

It is noted, in Figure 5c, that a strong edge state is formed at the *zigzag edge* termination of the *armchair* GNR depicted in Figure 5a. This implies a relatively high local density of charge and, in turn, high change of local potential (other bound states are present, but they are compensated by charge redistribution, similarly to what happened in the example of Figure 2).

The above edge mode occurs also in an *unperturbed* armchair GNR, but in that case, its charge contribution is halved by Fermi probability because its resonant energy is exactly zero (see inset of Figure 5a), consistent with the limit of guided modes in a very large zigzag GNR. When external voltages are applied or doping comes into play, so that the symmetry of occupied states is broken, this bound mode may be left out
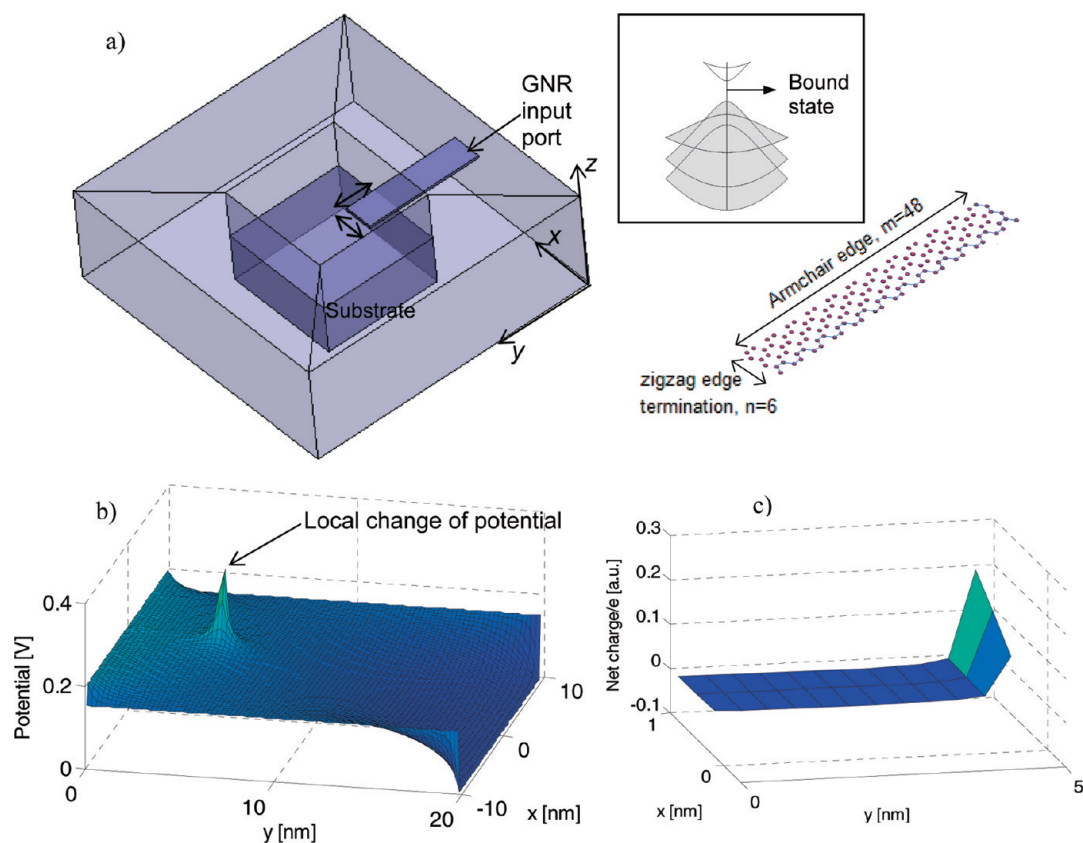
Figure 5. Simulation details: $n = 6$, $m = 48$, $V_g = 0.05$ V, $V_d = 0$ V, $V_s = 0.2$ V, Fermi level of contacted GNR = 0.6 eV, corresponding to a carrier density of ~2.6×10^{12} cm^{-2}; (a) simulated structure; (b) potential in the plane of the GNR; (c) net charge in the protruding GNR, each point of the curve represents four atomic sites.
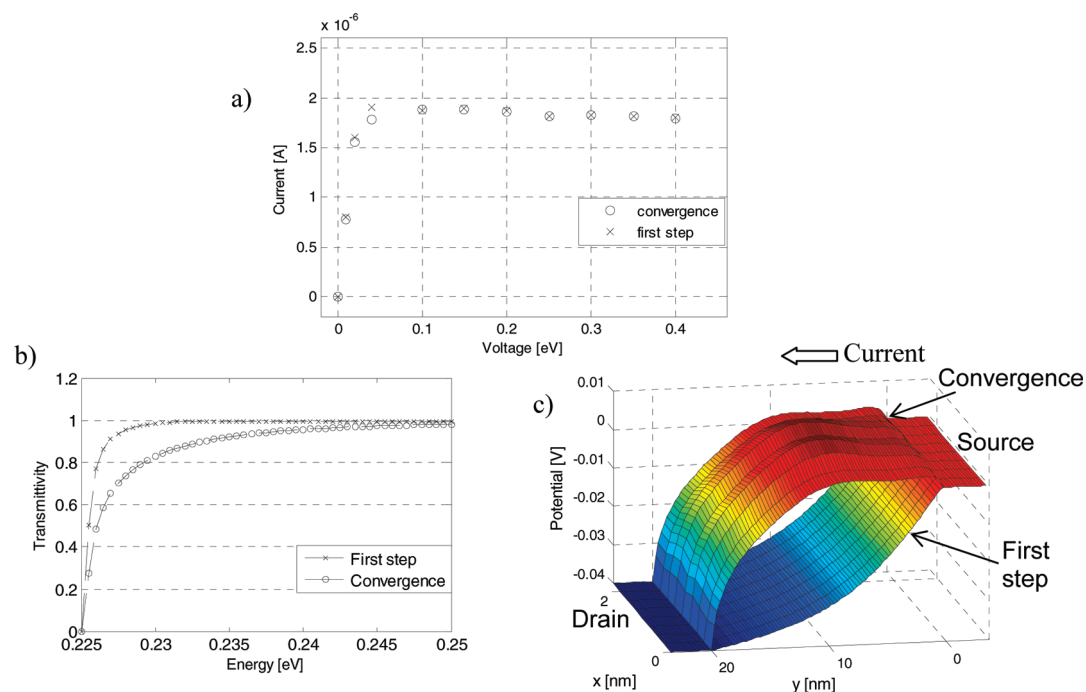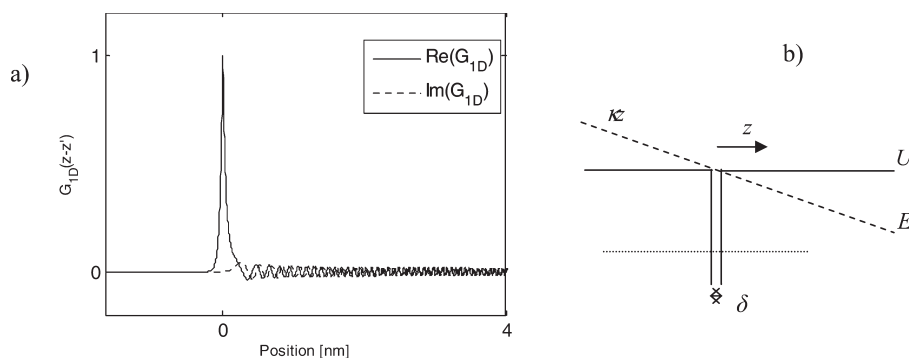

Figure 6. Simulation details: $n = 18$, $m = 184$, $V_g = 0$ V, Fermi level of contacted GNR = 0.25 eV, corresponding to a carrier density of ~9.6×10^{12} cm^{-2}. (a) Current–voltage characteristic. (b) Electron transmittivity from source to drain as a function of carrier energy. (c) Potential through the GNR with $V_d = -0.04$ and $V_s = 0$; the GNR on SiO$_2$ substrate extends from 0 to 20 nm in the y-direction.

Figure 7. (a) Example of G_{1D}: the strength of the electric field has been stressed to highlight the oscillating behavior; (b) potential profile in one-dimensional approximation of eq 9.

or fully included, depending on the sign of voltage or doping, in the charge balance (eq 8), causing a strong deviation from the unperturbed condition. We note, also, that the edge mode does not yield charge modulation, oscillation, or screening effects because of the large band gap and low charge density of the contacted GNR.

Numerical convergence is reached after three/four iterations. The same considerations of the previous subsection about numerical convergence still hold here. In addition, the following has to be remarked: the abrupt termination of the GNR makes the self-consistency somehow critical and the "equilibrium" of the final solution particularly unstable. This is likely to be true of any abrupt discontinuity of the GNR that implies strong local gradients of charge or potential. As a result, even small displacements from the final solution could prevent convergence. The applied iterative scheme requires a starting function for the potential, or for the charge, as close as possible to the final result.

In fact, the main issue in simulating complex nonlinear devices is given by handling the nonlinear Poisson–Schrödinger system. There is never any "*a priori*" guarantee that the iterative approach will actually converge to a stable solution. This is a rather common and well-known limit cycle problem, occurring when a particular charge density (Q_a) gives rise to a certain potential (V_a) and, in the next numerical cycle, a different pair (Q_b) and (V_b) is produced, so that charge and potential simply bounce back and forth from state **a** to state **b**, never converging. Moreover, small potential variations can strongly affect the charge density, due to the high number of modes involved, showing mode resonances and bound states. The inclusion of some loss mechanisms, such as phonon scattering, substrate effects, and a more rigorous treatment of the GNR–metal contact, is likely to lessen the strong coupling between potential and charge, thus reducing the instability domain.

Current Calculation in GNR. In the following example, we highlight the differences between the results obtainable by a self-consistent and a non-self-consistent approach. In particular, we consider a $n \cdot m = 18 \times 184$ atom armchair GNR deposited on SiO_2 and calculate the current (eq 6) driven by a source-to-drain voltage ranging from 0 to 0.4 V.

Figure 6a shows the current–voltage characteristic: crosses indicate currents computed non-self-consistently, whereas circles are self-consistent results. Interestingly, although the potential profile provided by a non-self-consistent approach, coinciding with the first step of the iterative calculation, may be considerably different from the self-consistent solution, corresponding to the convergence of the iterative calculation, the respective currents do not differ so much.

We have also reported, in Figure 6b,c, respectively, the electronic transmittivity through the GNR channel and the electrostatic potential, both calculated at $V_d = -0.04$ V and $V_s = 0$ V, that correspond to a point of appreciable discrepancy between the two curves of Figure 6a. In Figure 6b, energies are referred to the Fermi point of the GNR. As it is shown, the presence of a band gap Δ of about 0.45 eV allows significant transmittivity only at energies higher than $\Delta/2$. Again, in Figure 6b, crosses represent the first iteration step, whereas circles are for the last one. As a matter of fact, the two transmittivity curves do not differ very much; on the contrary, Figure 6c shows that the first-step potential is remarkably different from that of the last-step. This difference increases with the GNR charge density at metal contacts: here, the arbitrary value of 9.6×10^{12} cm^{-2} for the charge density has been assumed.

CONCLUSION

Multiport quantum transport in GNR has been analyzed by means of a scattering matrix approach. In this model, the charge density in GNR circuits is derived from a balance of carriers injected from ports and charges confined in electronic discrete states, and the computation is self-consistent with the self-generated and the externally applied electrostatic potentials. The possible formation of bound states has to be carefully considered, as it may have strong impact in

the calculations. We report examples of self-consistent simulation of GNR devices such as GNR-FETs and GNR

protrusions that could find interesting application as cold cathodes for X-ray generation.

COMPUTATIONAL METHODS

In this section, we propose an outline on field emission from GNR under an accelerating external potential. In all of the simulations, the GNR is considered as a defect-free lattice.

In general, the field emission depends on a variety of parameters, such as dimensionality, sharpness, work function/LDOS of the emitting object, and external fields. In the following, we suggest a method that could lead the way to an integration of charge transport and charge emission in a unified model.

We start from the source-free equation of a charge wave function ψ in a linear potential, and the corresponding one for the Green's function G

$$\left[\nabla^2 + \kappa z - \frac{2m}{\hbar^2}(U - E)\right]\psi = 0 \qquad (9a)$$

$$\left[\nabla^2 + \kappa z - \frac{2m}{\hbar^2}(U - E)\right]G = \delta(x - x')\delta(y - y')\delta(z - z') \qquad (9b)$$

where U is the vacuum energy, E is the charge energy, and $\kappa = 2m/\hbar^2 e\varepsilon$ accounts for the strength of the external electric field ε.

Cross multiplying by G and ψ, respectively, eqs 9a and 9b, subtracting the second equation from the first one, integrating over the volume V', and exploiting reciprocity, that is, $G(x',y',z',x,y,z) = G(x,y,z,x',y',z')$, yields

$$- \iint_{S'} \psi(x', y', z')\delta_{n'} G(x, y, z, x', y', z')$$

$$+ \iint_{S'} G(x, y, z, x', y', z')\delta_{n'} \psi(x', y', z') = \psi(x, y, z) \qquad (10)$$

where the normal derivatives are referred to the prime coordinates. The above equation is a familiar integral formulation of the differential problem 9a, often preferable for numerical reasons. As it could be readily verified, the Green's function can be expressed as

$$G(x, y, \bar{z}, x', y', \bar{z}') = \int_{-\infty}^{+\infty} \int_{-\infty}^{+\infty} e^{-jk_x(x - x')}e^{-jk_y(y - y')}G_{1D}(\bar{z}, \bar{z}')dk_x dk_y$$

$$(11)$$

where $= \kappa z - (k_x^2 + k_y^2) - 2m/\hbar^2(U - E)$, and G_{1D} is the one-dimensional Green's function solution of eq 9b with $\partial_x = -jk_x$, $\partial_y = -jk_y$.

If Green's function G_{1D} is properly chosen, that is, either it vanishes or its normal derivative vanishes or proper impedance conditions are satisfied at the boundaries, the problem is further simplified. In the present case, it is convenient to chose a Green function satisfying radiation conditions, assuming the form of outgoing traveling waves in the z-direction in terms of a proper combination of the Airy special functions: $Ai - jBi$, resulting from linear potential distribution. If the integration volume V' is assumed as the half space defined by the GNR plane, the contribution at infinity in the surface integrals (eq 10) vanishes because ψ and G_{1D} have the same functional form at infinity: in eq 10, only integrals on the GNR surface remain. In general, at large distance from the source point, we have

$$G_{1D} \propto \kappa^{-1/3}Ai(-\kappa^{-2/3}(\bar{z} - \bar{z}')) - j\kappa^{-1/3}Bi(-\kappa^{-2/3}(\bar{z} - \bar{z}'))$$

so that integration (eq 11) can be readily performed because each spectral component of Green's function is given by a

simple spatial shift of the one-dimensional Green's function. Within a one-dimensional approximation, the z-dependence of ψ in correspondence with a single atomic site, at any energy E, is assumed as that of a mode confined in a slab of thickness $\delta \sim 0.4$ nm away from vacuum level of an amount equal to $U - E$, as shown in Figure 7b. U and E refer to the Fermi level. The work function of the GNR is assumed to be similar to that of graphite, $\sim$4.6 eV. Using this approximation, the charge emitted by a single atomic site in the half spaces defined by the GNR plane can be calculated as

$$\psi(z > \delta/2) \approx - (\psi_s^0 \partial_{n'} G_{1D})|_{z' = \delta/2} + (G_{1D}\partial_{n'}\psi_s^0)|_{z' = \delta/2}$$

where the wave function and its z-derivative on the GNR surface are marked by the "0" apex to indicate the unperturbed case, that is, the absence of accelerating potential ($\kappa = 0$). The form of G_{1D} is shown explicitly in Figure 7a.

In general, of course, a more rigorous approach to the field emission problem requires the charge transport in the GNR plane (eq 2) to be coupled through an exchange Hamiltonian exploiting the Green's function 11 to the charge tunneling into the surroundings. Moreover, the electrostatic potential is typically a nonseparable function of (x,y,z), as it depends not only on the voltage applied at the electrodes (gate, drain, source, cathode, and anode) but also on the net charge distribution in the GNR. Engineering the field emission effect and the field enhancement factor from GNR, as well as evaluation of ionization potential of the system, are the subjects of ongoing work.

REFERENCES AND NOTES

1. Lin, Y.-M.; Dimitrakopoulos, C; Jenkins, K. A.; Farmer, D. B.; Chiu, H.-Y.; Grill, A.; Avouris, Ph. 100-GHz Transistors from Wafer-Scale Epitaxial Graphene. *Science* **2010**, *327*, 662.
2. Han, M. Y.; Özyilmaz, B.; Zhang, Y.; Kim, P. Energy Band-Gap Engineering of Graphene Nanoribbons. *Phys. Rev. Lett.* **2007**, *98*, 206805.
3. Li, X.; Wang, X.; Li, Z.; Lee, S. W.; Dai, H. Chemically Derived, Ultrasmooth Graphene Nanoribbon Semiconductors. *Science* **2008**, *319*, 1229–1232.
4. Stampfer, C.; Güttinger, J.; Hellmüller, S.; Molitor, F.; Ensslin, K.; Ihn, T. Energy Gaps in Etched Graphene Nanoribbons. *Phys. Rev. Lett.* **2009**, *102*, 056403.
5. Liu, X.; Oostinga, J. B.; Morpurgo, A. F.; Vandersypen, L. M. K. Electrostatic Confinement of Electrons in Graphene Nanoribbons. *Phys. Rev. B* **2009**, *80*, 121407.
6. Wakabayashi, K.; Sigrist, M. Zero-Conductance Resonances Due to Flux States in Nanographite Ribbon Junctions. *Phys. Rev. Lett.* **2000**, *84*, 3390–93.
7. Souma, S.; Ogawa, M.; Yamamoto, T; Watanabe, K. Numerical Simulation of Electronic Transport in Zigzag-Edged Graphene Nano-Ribbon Devices. *J. Comput. Electron.* **2008**, *7*, 390–393.
8. Brey, L.; Fertig, H. A. Electronic States of Graphene Nanoribbons Studied with the Dirac Equation. *Phys. Rev. B* **2006**, *73*, 235411.
9. Horing, N. J. M.; Liu, S. Y. Green's Functions for a Graphene Sheet and Quantum Dot in a Normal Magnetic Field. *J. Phys. A* **2009**, *42*, 225301.
10. Fiori, G.; Hong, S.; Iannacone, G.; Guo, G. J. Performance Comparison of Graphene Nanoribbon FETs with Schottky Contacts and Doped Reservoirs. *IEEE Trans. Electron. Devices* **2008**, *55*, 2314–2323.

11. Wang, Z. F.; Xiang, R.; Shi, Q. W.; Yang, J.; Wang, X.; Hou, J. G. Modeling STM Images in Graphene Using the Effective-Mass Approximation. *Phys. Rev. B* **2006**, *74*, 125417.

12. Ando, T. Quantum Point Contacts in Magnetic Fields. *Phys. Rev. B* **1991**, *44*, 8017–8027.

13. Castro, E. V.; Peres, N. M. R.; Lopes dos Santos, J. M. B. Gaped Graphene Bilayer: Disorder and Magnetic Field Effects. *Phys. Status Solidi B* **2007**, *244*, 2311–2316.

14. Rycerz, A. Nonequilibrium Valley Polarization in Graphene Nanoconstrictions. *Phys. Status Solidi A* **2007**, *205*, 1281–1289.

15. Akhmerov, A. R.; Beenakker, C. W. J. Boundary Conditions for Dirac Fermions on a Terminated Honeycomb Lattice. *Phys. Rev. B* **2008**, *77*, 085423.

16. Mencarelli, D.; Rozzi, T.; Pierantoni, L. Scattering Matrix Approach to Multichannel Transport in Many Lead Graphene Nanoribbons. *Nanotechnology* **2010**, *21*, 155701.

17. Mencarelli, D.; Rozzi, T.; Camilloni, C.; Maccari, L.; Donato, A. D.; Pierantoni, L. Modelling of Multi-wall CNT Devices by Self-Consistent Analysis of Multichannel Transport. *Nanotechnology* **2008**, *19*, 165202.

18. Eda, G.; Unalan, H. E.; Rupesinghe, N.; Amaratunga, G. A. J.; Chhowalla, M. Field Emission From Graphene Based Composite Thin Films. *Appl. Phys. Lett.* **2008**, *93*, 233502.

19. Bocharov, G. S.; Electskii, E. V.; Korshakov, A. V. Emission Characteristic of Carbon Nanotube-Based Cathodes. *Rev. Adv. Mater. Sci.* **2003**, *5*, 371–374.

20. Sharma, M.; Ghosh, S. Electron Transport and Goos-Hänchen Shift in Graphene with Electric and Magnetic Barriers: Optical Analogy and Band Structure. *J. Phys.: Condens. Matter* **2011**, *23*, 055501.

ARTICLE